SCIENTIFIC REPORTS

OPEN

SUBJECT AREAS:
NANOSCALE MATERIALS
MAGNETIC PROPERTIES AND MATERIALS
APPLIED PHYSICS

Received
21 February 2014

Accepted
26 June 2014

Published
22 July 2014

Correspondence and requests for materials should be addressed to Y.G.Z. (zhouyungang1@126.com); X.T.Z. (xtzu@uestc.edu.cn) or F.G. (Fei.Gao@pnnl.gov)

Evidencing the existence of intrinsic half-metallicity and ferromagnetism in zigzag gallium sulfide nanoribbons

Yungang Zhou[1], Sean Li[2], Weilie Zhou[3], Xiaotao Zu[1,4] & Fei Gao[5]

[1]School of Physical Electronics, University of Electronic Science and Technology of China, Chengdu, 610054, P.R. China, [2]School of Materials Science and Engineering, The University of New South Wales, Sydney, NSW 2052, Australia, [3]Advanced Materials Research Institute, University of New Orleans, New Orleans, LA 70148, USA, [4]Institute of Fundamental and Frontier Sciences, University of Electronic Science and Technology of China, Chengdu, 610054, P. R. China, [5]Pacific Northwest National Laboratory, MS K2-01, P.O. Box 999, Richland, Washington, 99352, USA.

The achievement of half-metallicity with ferromagnetic (FM) coupling has become a key technology for the development of one-dimensional (1D) nanoribbons for spintronic applications. Unfortunately, in previous studies, such a half-metallicity always occurs upon certain external constraints. Here we, for the first time, demonstrate, via density functional theory (DFT), that the recent experimentally realized gallium sulfide nanoribbons (GaSNRs) can display an intrinsic half-metallic character with FM coupling, raised from Ga-4*s*, Ga-4*p* and S-3*p* states at the Ga-dominated edge. Furthermore, the novel half-metallic behavior with FM coupling here is rather robust, especially for GaSNRs with large width and thickness, and can be sustained to the room temperature. Thus, our results accidentally disclose a new 1D spin nanomaterial, which allows us to go beyond the current scope limited to the graphene, boron nitride (BN), zinc oxide (ZnO) and molybdenum sulfide (MoS_2) nanoribbons, toward more realistic spintronic applications.

Since the discovery of 1D nanoribbons, it has sparked an intense research effect toward the understanding of such materials with the promising application in nano spintronic devices[1]. Nevertheless, such proposed application requires the ability of 100% spin-polarized at the Fermi level[2]. A half-metallicity can filter the current into a single spin channel, and thus fully meets this demand[3,4]. Consequently, the achievement of half-metallicity becomes the forefront of spintronics study.

To date, various strategies have been proposed theoretically to realize such 1D half-metallic nanostructure. Son et al. predicted the half-metallicity in zigzag graphene nanoribbon (GNR) under a sufficient transverse electric field across the ribbon[5]. This may open an exciting pathway to next-generation spintronics. However, in contrast to the widely applied gate voltage or bias electric fields in the current technology, the required transverse electric field for the half-metallicity transition increases with increasing ribbon width, and thus its realization is challenging[6]. To circumvent this difficulty, hydrogenation has also been proposed to realize the half-metallicity theoretically in GNR[7], while the experimental manipulation of hydrogen atoms to precise positions is still a challenge because hydrogen atoms are easy to form in a random way on a host surface. Recently, edge modification receives a lot of attentions due to the effective realization of half-metallicity in 1D nanostructures[8–13]. Although theoretical method seems successful in showing half-metallicity, it remains experimentally impractical because of the difficult in current edge micromanufacturing techniques. Another alternative approach to realize half-metallicity is to apply external strain. For example, the half-metallicity in MoS_2 nanoribbon (MoS_2NR) can occur when a tensile strain in zigzag direction arrives 11%[14]. However, the experimental achievement still represents a difficulty because the electronic and magnetic properties of MoS_2NR exhibit a very sensitive response to the applied strain that needs the fine control of strain on MoS_2NR. In fact, other various routes, such as injecting charges[15,16], doping atoms or organic molecules[17,18], inducing nanoholes[19,20], and hybriding different materials with the similar structure[6,21–24] also have been proposed to realize the novel half-metallicity in nanostructure, but an intrinsic half-metallicity without any external constraints is not yet demonstrated and is more desirable for the practical spintronic applications. In this respect, the effective acquisition of a 1D material with intrinsic half-metallic and FM character represents a key challenge to realize its practical application.

As a kind of 1D nanostructure, GaSNRs have been experimentally fabricated[25,26]. Shen et al. successfully synthesized high-quality 1D GaSNRs via a simple vapor-solid method, and pointed out that the morphology and structure of the products can be easily controlled by substrate temperature and evaporation source[25]. By a simple thermal

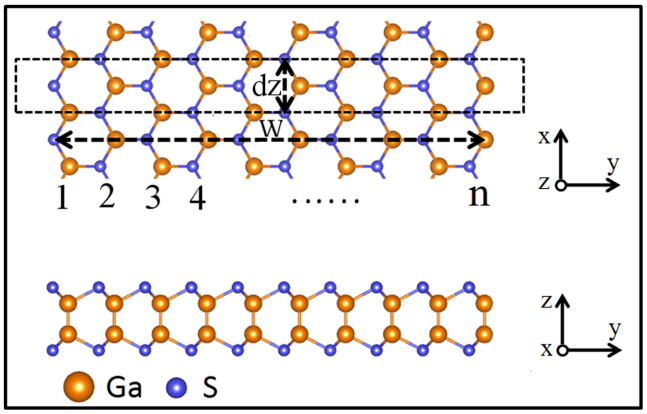

Figure 1 | Top and side views of the optimized geometric structure of $Z_{w=10,l=1}$-GaSNR. The ribbon is periodic along the x direction, and its width is denoted by w in the y direction. The region contained by the dashed rectangle is a unit cell used to calculate the magnetic moment, energy difference between AFM and FM couplings, and electronic properties.

evaporation process, the well-crystalline ultrathin GaSNRs have also been experimentally realized on silicon substrates, and are proposed as a promising electron source[26]. As a consequence, the experimental realization of GaSNRs might resolve the key challenge mentioned above. However, the scientific issue is if such GaSNRs can exhibit the intrinsic half-metallic character that has not been found in previous 1D nanostructures. If such a half-metallic property indeed exists, the effect from ribbon's width and thickness, especially at the room temperature, must be fully explored for practical applications. In order to unlock their valuable properties, a thorough understanding of structural, electronic, and spin properties of GaSNRs is highly desirable. However, to our best knowledge, the 1D GaSNRs with unique property have not yet received any theoretical attention so far.

In this paper, we explored the electronic and magnetic properties in a series of zigzag GaSNRs using DFT calculations, and found that all GaSNRs exhibit intrinsic half-metallic character. Moreover, the induced half-metallicity presents a substantial FM character through long-rang magnetic coupling, especially for GaSNRs with large width and thickness. Hence, our results provide a new pathway to explore GaSNRs-based spintronics. In contrast to previous studies, our results exhibit the following advantages over the existing ones: (1) it is not necessary to apply an external electric field or strain to GaSNRs, through which the half-metallicity can be found; (2) it is not necessary to induce point or line defects in GaSNRs, around which the half-metallicity may appear; (3) it is not necessary to modify the zigzag edge of GaSNRs by doping foreign atoms or organic molecules, near which the half-metallicity may be induced. Although these methods can be achieved experimentally, until now the effective manipulability at nanoscale is still a challenge.

Results

Geometries of zigzag GaSNRs. Our systematic study began with the geometric detail of a single gallium sulfide (GaS) layer. The perfect GaS layer is fourply with two Ga atoms in the middle which are covalently bonded to S atoms located in top and bottom sheets, forming S-Ga-Ga-S arrangement[27,28]. Computed lattice constant of 3.58 Å, S-Ga distance of 2.37 Å, and Ga-Ga distance of 2.46 Å are in good agreement with previous results[29,30]. The zigzag GaS nanoribbon (GaSNR) here was constructed by cutting the GaS layer along two parallel zigzag lines. For convenience, a zigzag GaSNR with a width of "n" and layers of "m" is described as $Z_{w=n,l=m}$-GaSNR. Figure 1 shows the top and side views of a fully relaxed $Z_{w=10,\ l=1}$-GaSNR (as an example). It is apparent that the honeycomb network and fourply structure in $Z_{w=10,l=1}$-GaSNR are well remained, supporting the experimental realization of such a GaSNR[25,26]. Previous studies have suggested that such unsaturated 1D nanoribbons are closely associated with magnetism[31–34]. Indeed, our calculations demonstrate that $Z_{w=10,l=1}$-GaSNR can lead to the magnetic moment of 0.753 μ_B. Here the unpaired spins of $Z_{w=10,l=1}$-GaSNR are mainly contributed by Ga (0.240 μ_B) and S (0.120 μ_B) atoms at the Ga-dominated edge, as shown in Figure 1S in the supplementary information. In contrast, no magnetism was found in all armchair GaSNRs, and thus we only consider zigzag GaSNRs in the following study of magnetic behaviors.

Half-metallicity of zigzag GaSNRs. One of the most interesting applications associated with the magnetism in nanoribbon is the novel half-metallicity. In order to explore if such a zigzag GaSNR can possess the novel half-metallic character in detail, we plot $Z_{w=10,l=1}$-GaSNR's spin-polarized band structure and density of states in Figure 2(a) and 2(b), respectively. Indeed a unique half-

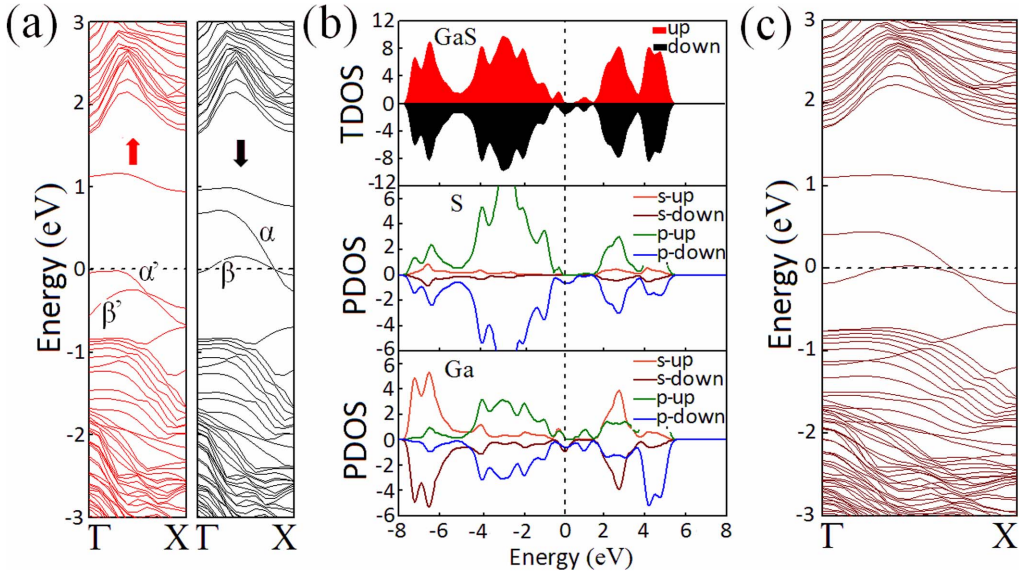

Figure 2 | (a) Spin-polarized band structure of $Z_{w=10,l=1}$-GaSNR, (b) spin-polarized total density of states (TDOS) of $Z_{w=10,l=1}$-GaSNR and projected density of states (PDOS) of Ga and S atoms and (c) spin-unpolarized band structure of $Z_{w=10,l=1}$-GaSNR. The Fermi level is set to zero.

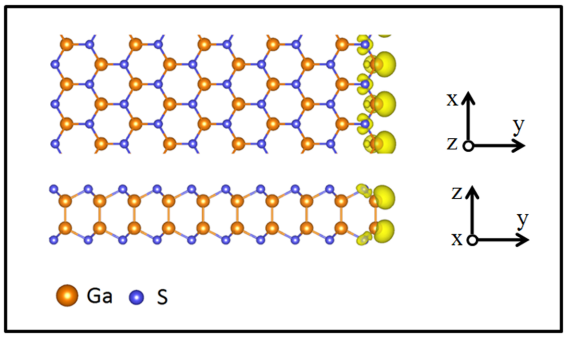

Figure 3 | Top and side views of spatial spin distribution of $Z_{w=10,l=1}$-GaSNR (isovalue 2 × 10^{-3} e/Å^3).

metallicity is observed. The spin-down electrons are metallic with two levels (α and β) crossing each other at the Fermi level while the spin-up electrons are semiconducting due to the existence of a band gap as large as 1.0 eV. The high spin polarization at the Fermi level can ensure a 100% passage of preferred spin, and it opens a transport channel only for spin-down electrons and blocks the channel for spin-up electrons. Thus, the charge transport is mainly dominated by the spin-down electrons. Considering the effect of edge passivation on the half-metallicity, we tested the passivation of Ga atoms at the Ga-dominated edge by H atoms. With H passivation, α and β levels in spin-down band can be kept well and the half-metallicity is nearly unchanged. The interesting result can be attributed to the composition of α and β levels. Here both α and β levels are composed not only by Ga-4*s* and Ga-4*p* but also by S-3*p* states. Thus, when Ga atoms were passivated by H atoms, α and β levels can still be kept well due to the existence of S-3*p* states. It is different to the result found in zigzag BN nanoribbons (BNNRs) where the half-metallic character can be somewhat affected by the passivation of N atoms at the N-dominated edge by H atoms[11]. In contrast, although previous studies also have predicated the half-metallicity upon certain external constraints mentioned above, such a half-metallicity without any external constraints here is intrinsic and thus should be more suitable for spin filter device applications. Considering the origin of special half-metallic character, we also calculated the spin-unpolarized band structure of $Z_{w=10,l=1}$-GaSNR in Figure 2(c). It can be seen that two half-filled states (HFSs) near the Fermi level were found. These HFSs near the Fermi level are zero-energy states, and the existence of degenerate HFSs is not stable. When the degree of freedom for spin is unrestricted, these half-filled HFSs split, and $Z_{w=10,l=1}$-GaSNR exhibits a half-metallic character. As a matter of fact, the achievement of half-metallicity due to half-filled HFSs has been demonstrated in previous study[35].

FM coupling of zigzag GaSNRs. To visualize the spin distribution of $Z_{w=10,l=1}$-GaSNR, we impose its spin density, i.e. the charge density difference between spin-up and spin-down channels, as shown in Figure 3. We can see that the unpaired spin almost concentrates on the Ga and S atoms in the Ga-terminated edge while the contribution from the inner and S-terminated edge atoms can be almost negligible agreeing with the magnetic moment's analysis in Figure 1S in the supplementary information. This is different to the finding in zigzag GNR and MoS_2NR where the unpaired spins are contributed from both edges[31,36], but similar to the result of zigzag ZnO nanoribbon (ZnONR) in which the unpaired spin is only contributed from the O-terminated edge[34]. The origin of unique spin distribution can be attributed to the Ga-S interaction. After relaxation, we found that the Ga-S bond length in the S-terminated edge was reduced by 0.15 Å, which results in the enhancement of the Ga-S covalent bonding interaction and thus quenches the magnetism of Ga and S atoms. Conversely, in the Ga-terminated edge, Ga-S bond length was slightly increased by 0.05 Å, resulting in the reduction of the Ga-S covalent bonding interaction and leading to the unpaired electrons accumulated on Ga and S atoms. In fact, the change of the magnetism due to the variation of covalent interaction is analogous to the result in previous studies[37,38]. Note that the unpaired spin electrons here align parallel, i.e. FM coupling, and exhibit a substantial collective character by long-range magnetic coupling. Considering the stability of such FM coupling, the energy difference between antiferromagnetic (AFM) and FM couplings needs to be further investigated. Figure 2S(a) in the supplementary information gives ten possible AFM couplings, i.e. AFMj ($1 \le j \le 10$), for monolayer GaSNRs. Calculated energy differences between AFM and FM couplings are about 18, 19, 17, 16, 18, 19, 20, 18, 18 and 20 meV

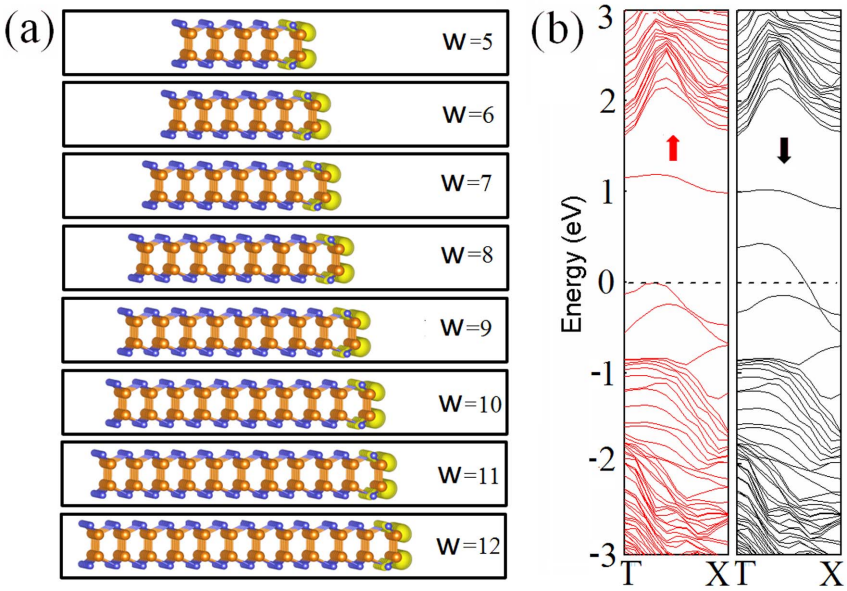

Figure 4 | (a) Front view of spatial spin distribution of $Z_{w=n,l=1}$-GaSNR ($5 \le n \le 12$) (isovalue 2 × 10^{-3} e/Å^3) (b) spin-polarized band structure of $Z_{w=12,l=1}$-GaSNR. Note that the spin-polarized band structure of $Z_{w=n,l=1}$-GaSNR ($5 \le n \le 11$) presents the similar half-metallic character that was not given. The Fermi level is set to zero.

Table I | Magnetic moments of FM and AFM couplings and energy difference between AFM and FM couplings per unit cell for a series of $Z_{w=n,l=1}$-GaSNRs ($5 \le n \le 12$, 20). Here M_{FM} and M_{AFMj} ($1 \le j \le 10$) denote magnetic moment of FM and AFMj couplings, respectively. ΔE_j ($1 \le j \le 10$) denotes the energy difference between AFMj ($1 \le j \le 10$) and FM couplings

Width (n)	5	6	7	8	9	10	11	12	20
M_{FM} (μ_B)	0.703	0.713	0.721	0.732	0.742	0.753	0.773	0.781	0.794
M_{AFM1} (μ_B)	0.452	0.457	0.461	0.468	0.473	0.481	0.485	0.492	0.510
M_{AFM2} (μ_B)	0.215	0.221	0.225	0.232	0.236	0.242	0.248	0.254	0.262
M_{AFM3} (μ_B)	0.000	0.000	0.000	0.000	0.000	0.000	0.000	0.000	0.000
M_{AFM4} (μ_B)	0.212	0.217	0.225	0.232	0.237	0.241	0.246	0.254	0.263
M_{AFM5} (μ_B)	0.000	0.000	0.000	0.000	0.000	0.000	0.000	0.000	0.000
M_{AFM6} (μ_B)	0.000	0.000	0.000	0.000	0.000	0.000	0.000	0.000	0.000
M_{AFM7} (μ_B)	0.000	0.000	0.000	0.000	0.000	0.000	0.000	0.000	0.000
M_{AFM8} (μ_B)	0.000	0.000	0.000	0.000	0.000	0.000	0.000	0.000	0.000
M_{AFM9} (μ_B)	0.000	0.000	0.000	0.000	0.000	0.000	0.000	0.000	0.000
M_{AFM10} (μ_B)	0.000	0.000	0.000	0.000	0.000	0.000	0.000	0.000	0.000
ΔE_1 (meV)	18	20	24	25	28	33	35	38	40
ΔE_2 (meV)	19	21	25	27	29	34	37	40	41
ΔE_3 (meV)	17	18	20	22	24	29	30	33	35
ΔE_4 (meV)	16	18	20	23	26	28	29	32	35
ΔE_5 (meV)	18	20	22	26	29	33	34	35	36
ΔE_6 (meV)	19	21	25	26	29	34	36	40	41
ΔE_7 (meV)	20	22	27	28	30	35	38	41	43
ΔE_8 (meV)	18	19	22	23	25	31	32	34	36
ΔE_9 (meV)	18	19	21	24	27	29	31	33	36
ΔE_{10} (meV)	20	21	23	28	30	34	36	37	38

for AFM1, AFM2, AFM3, AFM4, AFM5, AFM6, AFM7, AFM8, AFM9 and AFM10, respectively. Here calculated energy differences between AFM and FM couplings are based on a unit cell as shown in Figure 1. These results suggest that FM coupling is more stable than AFM coupling for all cases considered. Conventionally, the induced magnetism is often located on adsorbed atoms or near vacant sites. However, for a doped system, one of the crucial issues for its applications in spintronic devices is whether the local spin moments induced by defect states can lead to a collective magnetism, which is an essential requirement for any spintronic applications. Unfortunately, this critical issue, as well as its implications, was often overlooked in the previous studies of the doping-induced magnetism of nanostructures. Here the finding of FM spin coupling with a substantial collective character renders GaSNR a more practical candidate for spintronic applications.

Influence of ribbon width on half-metallicity and FM coupling. Since experimentally synthesized nanoribbons always have a relative large width, we investigated the width effect on the electronic and magnetic properties on zigzag GaSNR. Interestingly, from our calculations, zigzag GaSNR with a large width still exhibits the half-metallic character with FM coupling. The relevant spatial spin distributions and the spin-polarized band structure are given in Figure 4(a) and 4(b), respectively. The interesting result can be attributed to the stable edge structure which dominates the half-metallic character and is independent of the GaSNR width. In order to further understand coupling behaviors, we calculated magnetic moments of FM and AFM couplings and energy difference between AFM and FM couplings for GaSNR with different width, as shown in Table I. It can be seen that FM coupling is more stable than AFM coupling for all cases

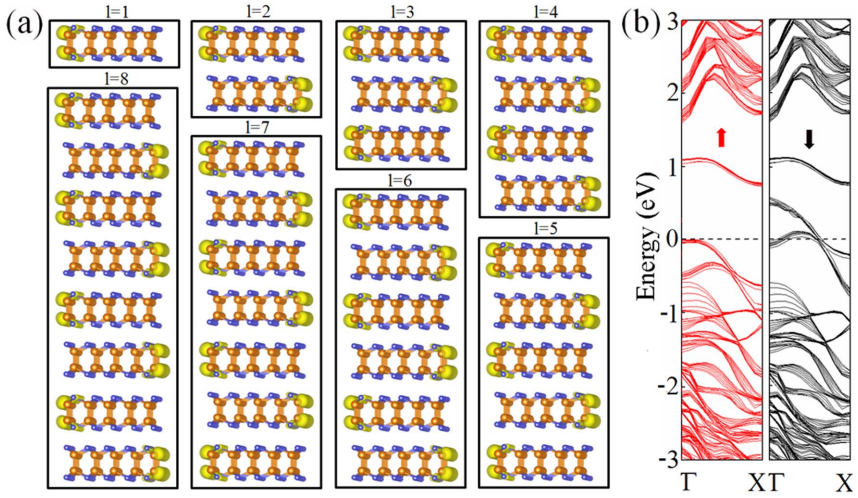

Figure 5 | (a) Front view of spatial spin distribution of $Z_{w=5,l=m}$-GaSNR ($1 \le m \le 8$) (isovalue 2×10^{-3} e/Å^3) (b) spin-polarized band structure of $Z_{w=5,l=8}$-GaSNR. Note that the spin-polarized band structure of $Z_{w=5,l=m}$-GaSNR ($1 \le m \le 7$) presents the similar half-metallic character that was not given. The Fermi level is set to zero.

Table II | Magnetic moments of FM and AFM couplings and energy difference between AFM and FM couplings per unit cell for a series of $Z_{w=5,l=m}$-GaSNRs ($1 \le m \le 8$). Here M_{FM} and M_{AFMj} ($1 \le j \le 10$) denote magnetic moment of FM and AFMj couplings, respectively. ΔE_j ($1 \le j \le 10$) denotes the energy difference between AFMj ($1 \le j \le 10$) and FM couplings

Layer (m)	1	2	3	4	5	6	7	8
M_{FM} (μ_B)	0.703	1.502	2.230	2.925	3.624	4.361	5.121	5.725
M_{AFM1} (μ_B)	0.452	0.904	1.354	1.801	2.261	2.712	3.165	3.615
M_{AFM2} (μ_B)	0.215	0.431	0.645	0.865	1.078	1.286	1.509	1.725
M_{AFM3} (μ_B)	0.000	0.000	0.000	0.000	0.000	0.000	0.000	0.000
M_{AFM4} (μ_B)	0.212	0.425	0.635	0.864	1.084	1.310	1.482	1.695
M_{AFM5} (μ_B)	0.000	0.000	0.000	0.000	0.000	0.000	0.000	0.000
M_{AFM6} (μ_B)	0.000	0.000	0.000	0.000	0.000	0.000	0.000	0.000
M_{AFM7} (μ_B)	0.000	0.000	0.000	0.000	0.000	0.000	0.000	0.000
M_{AFM8} (μ_B)	0.000	0.000	0.000	0.000	0.000	0.000	0.000	0.000
M_{AFM9} (μ_B)	0.000	0.000	0.000	0.000	0.000	0.000	0.000	0.000
M_{AFM10} (μ_B)	0.000	0.000	0.000	0.000	0.000	0.000	0.000	0.000
ΔE_1 (meV)	18	37	56	74	94	115	136	157
ΔE_2 (meV)	19	39	60	81	102	122	142	162
ΔE_3 (meV)	17	35	55	73	92	112	130	151
ΔE_4 (meV)	16	33	51	72	90	111	129	147
ΔE_5 (meV)	18	37	55	73	95	116	136	156
ΔE_6 (meV)	19	39	58	76	95	115	135	153
ΔE_7 (meV)	20	40	62	81	102	123	142	163
ΔE_8 (meV)	18	37	55	72	91	108	128	146
ΔE_9 (meV)	18	37	54	73	72	107	128	148
ΔE_{10} (meV)	20	41	62	83	103	125	145	165

considered. For FM coupling, $Z_{w=5,l=1}$-GaSNR has a lowest magnetic moment with the relatively low energy difference, and $Z_{w=20,l=1}$-GaSNR has a largest magnetic moment with the relatively large energy difference. It is expected that magnetic moment and energy difference increase with the ribbon width, indicating that not only the magnetic moment of FM coupling but also the stability of FM coupling are enhanced with the increase of the ribbon width. However, no magnetism is found from the calculation of infinitely single-layered GaS because the magnetic moment per GaS molecular formula decreases with the increase of width, which is analogous to that studied previously in MoS_2NR[31]. Nevertheless, the experimentally synthesized GaSNRs with large width are expected to possess very large magnetic moment and stability for FM coupling and thus are expected for practical applications.

Influence of ribbon thickness on half-metallicity and FM coupling. Since the experimentally synthesized nanoribbons generally consist of several layers, we also considered the thickness effect on the electronic and magnetic properties of zigzag GaSNRs. Here the width of GaSNR was fixed to be w = 5 for computational expediency and a multilayer ribbon was constructed by placing the planar layers on top of each other with an AB stacking. As noted in Figure 5(a) and 5(b), the spin density of $Z_{w=5,l=m}$-GaSNR can be viewed as a simple combination of those in $Z_{w=5,l=1}$-GaSNRs, and even with more layers zigzag GaSNR still presents a half-metallic character. As a comparison, zigzag ZnONR exhibits a different behavior, where the edge atoms of the top layer can covalently bind with the edge atoms of the bottom layer and thus the magnetism diminishes when the number of layers becomes even[34]. This interesting result may be attributed to the very weak van der Waals interaction between GaSNRs where the average separation between two neighboring GaSNRs is about 3.4 Å. In order to further understand coupling behaviors, we calculated magnetic moments of FM and AFM couplings and energy difference between AFM and FM couplings for GaSNR with different thickness, as shown in Table II. Here ten possible AFM couplings, i.e. AFMj ($1 \le j \le 10$), for multilayer GaSNRs are shown in Figure 2S(b) in the supplementary information. It can be seen that FM coupling are more stable than AFM coupling for all cases considered. For FM coupling, calculated magnetic moment for $Z_{w=5,l=m}$-GaSNR structure can be approximately determined to be 0.703 m μ_B, and calculated energy difference between AFM and FM couplings for $Z_{w=5,l=m}$-GaSNR structure can be approximately evaluated to be 18 m, 19 m, 17 m, 16 m, 18 m, 19 m, 20 m, 18 m, 18 m and 20 m meV for AFM1, AFM2, AFM3, AFM4, AFM5, AFM6, AFM7, AFM8, AFM9 and AFM10, respectively. It indicates that the experimentally synthesized GaSNRs with large number of layers are expected to possess very large magnetic moment and stability for FM coupling and thus are expected for practical applications.

Influence of temperature on half-metallicity and FM coupling. Considering whether the experimentally fabricated GaSNRs can be served at room temperature, spin-polarized molecular dynamics (MD) simulations were carried out for 1 fs at 300 K. Figure 6 depicts the fluctuation of the total energy (E_{tot}) and the magnetic moment (M) of three representative GaSNRs, i.e., $Z_{w=5,l=1}$-, $Z_{w=12,l=1}$- and $Z_{w=5,l=8}$-GaSNRs, as a function of time. We found that, after 2000 steps, the geometries of three configurations still remain, but with small variations in total energy and magnetic moment. This can be rationalized by the fact that the Ga-S binding energies in GaSNRs are much larger than the thermal energy corresponding to the room temperature. As a consequence, GaSNRs still exhibit half-metallic character with FM coupling. (Note that half-metallic character and FM coupling here were determined by DFT simulations at 0 K with the configuration obtained from MD simulations at room temperature.) Hence, the novel half-metallic character, along with FM coupling, renders the GaSNRs an excellent candidate for spintronic applications at room temperature.

Influence of calculated functional on half-metallicity and FM coupling. For the exchange-correlation functional, DFT calculated band gaps are generally lower than experimentally determined band gaps. Hence, we have tested band structures in a series of zigzag GaSNRs with Heyd-Scuseria-Ernzerhof (HSE06) hybrid functional. Although HSE06 calculated band structures are somewhat different from those by DFT calculation, HSE06 calculation also gives the similar magnetic behaviors, i.e. half-metallicity and FM coupling. Hence, our calculated results survive to the choice of functional.

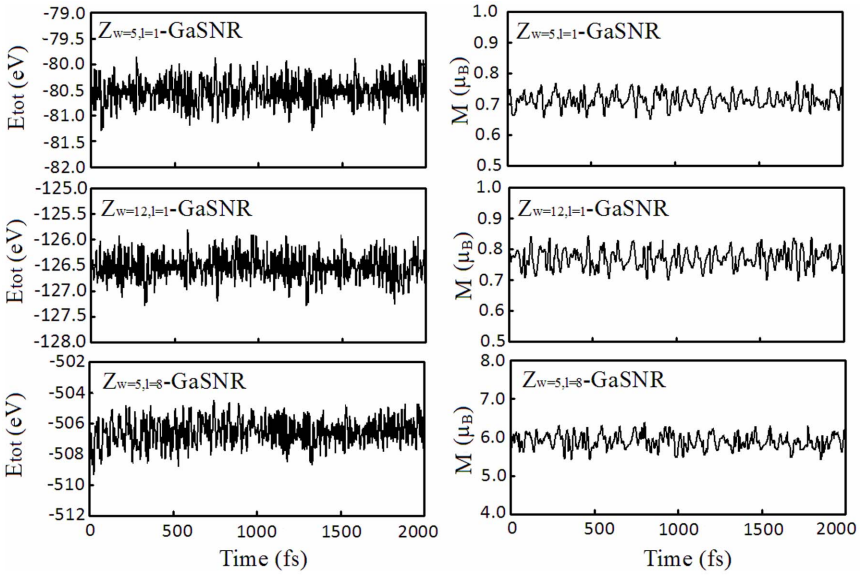

Figure 6 | The variation of the total energies, E_{tot}, and the magnetic moment, M, with time from molecular dynamics simulations for $Z_{w=5,l=1}$-, $Z_{w=12,l=1}$- and $Z_{w=5,l=8}$-GaSNRs.

Discussion

Half-metallicity with FM coupling has become a key technology for 1D nanostructure's application in spintronics. Previously, such a half-metallicity always occurs under certain external constraints, such as applying an external electric field or strain, inducing point or line defects, as well as modifying the zigzag edge. Nonetheless, considering the practical spintronic applications, the effective acquisition of an intrinsic half-metallicity without any external constraints is particularly important, which represents a significant challenge for modern technologies. Based on spin-polarized DFT, we, for the first time, demonstrated the existence of intrinsic half-metallicity with FM coupling in recent experimentally realized GaSNRs. Although corresponding AFM couplings present metallic character as shown in Figure 3S in the supplementary information, the unique half-metallic character with FM coupling here is more stable than metallic character with AFM couplings, especially for experimentally realized GaSNRs with large width and thickness. Furthermore, the novel half-metallic behavior with FM coupling can be sustained to the room temperature. Thus, our results accidentally disclose a new 1D spin nanomaterial toward the more realistic spintronic applications. In contrast to previous studies, our results exhibit the following advantages over the existing ones: (1) we do not need to apply an external electric field or strain in GaSNRs to realize their half-metallicity; (2) we do not need to induce point or line defects in GaSNRs to realize their half-metallicity; (3) also, we do not need to modify the zigzag edge of GaSNRs by foreign atoms or organic molecules to realize their half-metallicity. Although these methods can been achieved experimentally, until now the effective manipulability at nanoscale is still a challenge.

Methods

The first principle periodic calculations based on DFT are performed using the Vienna *ab initio* simulation package (VASP). Within generalized gradient approximation (GGA), we considered Perdew−Burke−Ernzerhof (PBE) exchange and correlation functional. The pseudopotentials with $4s^24p^1$ and $3s^23p^4$ valence electron configurations are used for Ga and S atoms, respectively. The electronic wave functions were expanded using a plane-wave basis set with a cutoff energy of 350 eV. The Brillouin zone was sampled by 20 special *k* points for atomic structure relaxation and 30 *k* points for the electronic structure calculation. A 1D periodic boundary condition was applied along the ribbon. Both of vacuum distances between ribbon edges and between layers of two adjacent images are set to be about 10 Å. Full optimization of the atomic structures including the atomic positions and lattice parameters has been carried until all the force components are smaller than 0.01 eV/Å, and the convergence of the electronic self-consistent energy is less than 10^{-5} eV. DFT calculated band gaps are generally lower than experimentally determined band gaps, and thus HSE06 hybrid functional also has been used to verify the correctness of electronic and magnetic properties of zigzag GaSNRs. HSE06's results show that major magnetic behaviors, i.e. half-metallicity and FM coupling in zigzag GaSNRs, are similar to those found from DFT calculation.

1. Wolf, S. A. *et al.* Spintronics: a Spin-based Electronics Vision for the Future. *Science* **294**, 1488–1495 (2001).
2. Prinz, G. A. Magnetoelectronics. *Science* **282**, 1660–1663 (1998).
3. Keizer, R. S. *et al.* A Spin Triplet Supercurrent through the Half-metallic Ferromagnet CrO_2. *Nature* **439**, 825–827 (2006).
4. Du, A., Sanvito, S. & Smith, S. C. First-principles Prediction of Metal-free Magnetism and Intrinsic Half-Metallicity in Graphitic Carbon Nitride. *Phys. Rev. Lett.* **108**, 197207 (2012).
5. Son, Y. W., Cohen, M. L. & Louie, S. G. Half-metallic Graphene Nanoribbons. *Nature* **444**, 347–349 (2006).
6. Yu, J. & Guo, W. L. A New Paradigm to Half-metallicity in Graphene Nanoribbons. *J. Phys. Chem. Lett.* **4**, 951–955 (2013).
7. Zhou, Y. G. *et al.* Hydrogenated Graphene Nanoflakes: Semiconductor to Half-metal Transition and Remarkable Large Magnetism. *J. Phys. Chem. C* **116**, 5531–5537 (2012).
8. Kan, E. J., Li, Z. Y., Yang, J. L. & Hou, J. G. Half-metallicity in Edge-modified Zigzag Graphene Nanoribbons. *J. Am. Chem. Soc.* **130**, 4224–4225 (2008).
9. Wu, M. H., Wu, X. J., Gao, Y. & Zeng, X. C. Materials Design of Half-metallic Graphene and Graphene Nanoribbons. *Appl. Phys. Lett.* **94**, 223111 (2009).
10. Hod, O., Barone, V., Peralta, J. E. & Scuseria, G. E. Enhanced Half-metallicity in Edge-oxidized Zigzag Graphene Nanoribbons. *Nano Lett.* **7**, 2295–2299 (2007).
11. Zheng, F. W. *et al.* Half Metallicity along the Edge of Zigzag Boron Nitride Nanoribbons. *Phys. Rev. B* **78**, 205415 (2008).
12. Wang, Y. L., Ding, Y. & Ni, J. Fluorination-induced Half-metallicity in Zigzag Boron Nitride Nanoribbons: First-principles Calculations. *Phy. Rev. B* **81**, 193407 (2010).
13. Chen, Q., Zhu, L. Y. & Wang, J. L. Edge-passivation Induced Half-metallicity of Zigzag Zinc Oxide Nanoribbons. *Appl. Phys. Lett.* **95**, 133116 (2009).
14. Kou, L. Z. *et al.* Tuning Magnetism and Electronic Phase Transitions by Strain and Electric Field in Zigzag MoS_2 Nanoribbons. *J. Phys. Chem. Lett.* **3**, 2934–2941 (2012).
15. Wu, M. H., Zhang, Z. H. & Zeng, X. C. Charge-injection Induced Magnetism and Half Metallicity in Single-layer Hexagonal Group III/V (BN, BP, AlN, AlP) Systems. *Appl. Phys. Lett.* **97**, 093109 (2010).
16. Menezes, M. G. & Capaz, R. B. Half-metallicity Induced by Charge Injection in Hexagonal Boron Nitride Clusters Embedded in Graphene. *Phys. Rev. B* **86**, 195413 (2012).
17. Lee, Y. L., Kim, S., Park, C., Ihm, J. & Son, Y. W. Controlling Half-metallicity of Graphene Nanoribbons by Using a Ferroelectric Polymer. *ACS Nano* **4**, 1345–1350 (2012).
18. Krasheninnikov, A. V., Lehtinen, P. O., Foster, A. S., Pyykkö, P. & Nieminen, R. M. Embedding Transition-metal Atoms in Graphene: Structure, Bonding, and Magnetism. *Phys. Rev. Lett.* **102**, 126807 (2009).

19. Du, A. J. *et al.* C-BN Dots versus Antidots: Computational Exploration of Structure, Magnetism, and Half-metallicity in Boron-nitride Nanostructures. *J. Am. Chem. Soc.* **131**, 17354–17359 (2009).
20. Kan, E. J. *et al.* Half-metallicity in Organic Single Porous Sheets. *J. Am. Chem. Soc.* **134**, 5718–5721 (2012).
21. Du, A. J., Chen, Y., Zhu, Z. H., Lu, G. Q. & Smitht, S. C. C-BN Single-walled Nanotubes from Hybrid Connection of BN/C Nanoribbons: Prediction by ab initio Density Functional Calculations. *J. Am. Chem. Soc.* **131**, 1682–1683 (2009).
22. Huang, B. *et al.* Intrinsic Half-metallic BN-C nanotubes. *Appl. Phys. Lett.* **97**, 043115 (2010).
23. Dutta, S., Manna, A. K. & Pati, S. K. Intrinsic Half-metallicity in Modified Graphene Nanoribbons. *Phys. Rev. Lett.* **102**, 096601 (2009).
24. Pruneda, J. M. Origin of Half-semimetallicity Induced at Interfaces of C-BN Heterostructures. *Phys. Rev. B* **81**, 161409 (2010).
25. Shen, G. Z., Chen, D., Chen, P. C. & Zhou, C. W. Vapor-solid Growth of One-dimensional Layer-structured Gallium Sulfide Nanostructures. *ACS Nano* **3**, 1115–1120 (2009).
26. Panda, S. K. *et al.* Synthesis of Well-crystalline GaS Nanobelts and Their Unique Field Emission Behavior. *J. Phys. Chem. C* **112**, 6240–6244 (2008).
27. Late, D. J., Liu, B., Matte, H., Rao, C. N. R. & Dravid, V. P. Rapid Characterization of Ultrathin Layers of Chalcogenides on SiO_2/Si Substrates. *Adv. Funct. Mater.* **22**, 1894–1905 (2012).
28. Hu, P. A. *et al.* Highly Responsive Ultrathin GaS Nanosheet Photodetectors on Rigid and Flexible Substrates. *Nano Lett.* **13**, 1649–1653 (2013).
29. Ding, Y. & Wang, Y. Electronic Structures of Silicene/GaS Heterosheets. *Appl. Phys. Lett.* **103**, 043114 (2013).
30. Ma, Y. D., Dai, Y., Guo, M., Yu, L. & Huang, B. B. Tunable Electronic and Dielectric Behavior of GaS and GaSe Monolayers. *Phys. Chem. Chem. Phys.* **15**, 7098–7105 (2013).
31. Li, Y. F., Zhou, Z., Zhang, S. B. & Chen, Z. F. MoS_2 Nanoribbons: High Stability and Unusual Electronic and Magnetic Properties. *J. Am. Chem. Soc.* **130**, 16739–16744 (2008).
32. Wu, W. Z., Lu, P., Zhang, Z. H. & Guo, W. L. Electronic and Magnetic Properties and Structural Stability of BeO Sheet and Nanoribbons. *ACS Appl. Mater. Interfaces* **3**, 4787–4795 (2011).
33. Lai, L. *et al.* Magnetic Properties of Fully Bare and Half-bare Boron Nitride Nanoribbons. *J. Phys. Chem. C* **113**, 2273–2276 (2009).
34. Botello-Mendez, A. R., Lopez-Urias, F., Terrones, M. & Terrones, H. Magnetic Behavior in Zinc Oxide Zigzag Nanoribbons. *Nano Lett.* **8**, 1562–1565 (2008).
35. Yu, S. S., Zheng, W. T., Wang, C. & Jiang, Q. Nitrogen/Boron Doping Position Dependence of the Electronic Properties of a Triangular Graphene. *ACS Nano* **4**, 7619–7629 (2010).
36. Son, Y. W., Cohen, M. L. & Louie, S. G. Energy Gaps in Graphene Nanoribbons. *Phys. Rev. Lett.* **97**, 216803 (2006).
37. Ma, Y. D. *et al.* Evidence of the Existence of Magnetism in Pristine VX_2 Monolayers (X = S, Se) and Their Strain-induced Tunable Magnetic Properties. *ACS Nano* **6**, 1695–1701 (2012).
38. Zhou, Y. G. *et al.* Tensile Strain Switched Ferromagnetism in Layered NbS_2 and $NbSe_2$. *ACS Nano* **6**, 9727–9736 (2012).

Acknowledgments

We thank Chundong Wang and Wei Liu for useful discussions of this work.

Author contributions

Y.G.Z. proposed the idea, performed calculations and wrote the manuscript. X.T.Z. and F.G. discussed the results. S.L. and W.L.Z. revised the paper.

Additional information

Supplementary information accompanies this paper at http://www.nature.com/scientificreports

Competing financial interests: The authors declare no competing financial interests.

How to cite this article: Zhou, Y.G., Li, S., Zhou, W.L., Zu, X.T. & Gao, F. Evidencing the existence of intrinsic half-metallicity and ferromagnetism in zigzag gallium sulfide nanoribbons. *Sci. Rep.* **4**, 5773; DOI:10.1038/srep05773 (2014).